

Part Segmentation and Motion Estimation for Articulated Objects with Dynamic 3D Gaussians

Jun-Jee Chao¹
chao0107@umn.edu

Qingyuan Jiang¹
jian0345@umn.edu

Volkan Isler²
isler@cs.utexas.edu

¹ Department of Computer Science
University of Minnesota
Minnesota, USA

² Department of Computer Science
The University of Texas at Austin
Texas, USA

Abstract

Part segmentation and motion estimation are two fundamental problems for articulated object modeling. In this paper, we present a method to solve these two problems jointly from a sequence of observed point clouds of a single articulated object. The main challenge in our problem setting is that the point clouds are not assumed to be generated by a fixed set of moving points. Instead, each point cloud in the sequence could be an arbitrary sampling of the object surface at that particular time step. Such scenarios occur when the object undergoes major occlusions, or if the dataset is collected using measurements from multiple sensors asynchronously. In these scenarios, methods that rely on tracking point correspondences are not appropriate. We present an alternative approach by representing the object as a collection of simple building blocks modeled as 3D Gaussians. With our representation, part segmentation is achieved by assigning the observed points to the Gaussians. Moreover, the transformation of each point across time can be obtained by following the poses of the assigned Gaussian. Experiments show that our method outperforms existing methods that solely rely on finding point correspondences. Additionally, we extend existing datasets to emulate real-world scenarios by considering viewpoint occlusions. We demonstrate that our method is more robust to missing points as compared to existing approaches on these challenging datasets, even when some parts are completely occluded in some time-steps. Notably, our part segmentation outperforms the state-of-the-art method by 13% on occluded point clouds. Project page: https://giles200619.github.io/gsmart_website/

1 Introduction

Identifying rigid parts and motions of articulated objects is fundamental for building digital twins [14], object re-posing [34], and system identification in robotics [10, 49]. However, building articulated models from point cloud sequences is challenging. In real-world scenarios, such sequences are usually captured from multiple sensors asynchronously. This data collection process leads to the main challenge: the observed point cloud sequence is not generated by a fixed set of moving points. Instead, each point cloud in the sequence could be an

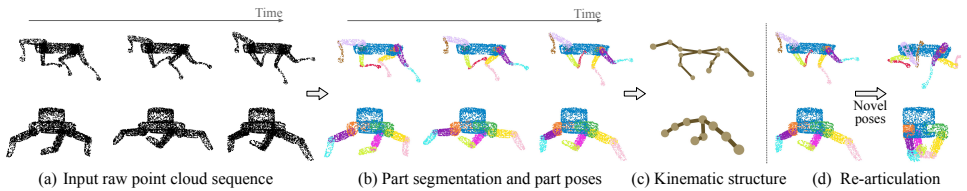


Figure 1: Problem formulation: (a) Given a dynamic point cloud sequence of an articulated object, (b-c) the goal is to jointly estimate per-frame part segmentation, part poses, and the kinematic structure with joint parameters. (d) The estimated model can both reconstruct the observed motion and re-articulate the object to novel, unseen poses. Note that our method makes no assumptions about object category, kinematic structure, or number of parts.

arbitrary sampling of the object surface at that particular time step. Therefore, corresponding points might not exist across the observed sequence. The problem becomes even harder under occlusions caused by varying sensor locations at each time step. With only a single sensor, different parts of the object become invisible in different time steps. Hence, methods that rely solely on point correspondences often struggle under these conditions [12, 26].

Instead of relying solely on point correspondences, we propose an alternative approach to jointly estimate a) part segmentation, b) kinematic tree, and c) joint poses directly from a raw point cloud sequence of a single articulated object (Fig. 1). Our method represents the articulated object as a set of dynamic 3D Gaussians, where each Gaussian models the motion and point distribution of a rigid part. A key component of our method is the Gaussian parametrization technique inspired by the success of Gaussian Splatting [18, 31], where we parameterize each Gaussian with time-varying rotations and translations, while sharing scales across time. This compact representation enables efficient part segmentation, motion estimation, and point transformation with minimal parameters. Moreover, the estimated parameters can be used to re-articulate the object to a new pose that has not been seen before.

Unlike many existing methods, we do not make any assumption about the object category [3, 8, 21, 28, 30, 32], number of parts [11, 12, 13, 15, 24, 47], or the underlying kinematic tree structure [22, 33, 34, 38], therefore making our method more generalizable to in-the-wild objects and more suitable for real-world applications. We show in Section 4 that our method outperforms existing works on two established benchmarks. Furthermore, while existing approaches focus on point clouds that fully cover the object surface, less attention has been given to modeling point cloud sequences with occlusions. To assess performance under such conditions, we extend the dataset to mimic real-world scenario by involving viewpoint occlusions. Experiment results show that our method is more robust to missing points in the observed point clouds compared to existing works. Our contributions can be summarized as:

- To build an articulated model from raw 4D point cloud of an arbitrary articulated object, we present a compact and effective representation by modeling rigid part segmentation and motion with dynamic 3D Gaussians.
- Compared to most existing point cloud-based methods that solely rely on point correspondence, our method that considers point distribution outperforms existing methods on established benchmarks.
- We study the performance of our method when the input point clouds undergo occlusions. Experiments show that our method is more robust to missing points than existing approaches. Notably, our part segmentation outperforms the state-of-the-art (SoTA) method by 13% on point clouds with partial observations.

2 Related Work

Object part segmentation. Many methods perform part segmentation on static point clouds using deep learning [23, 25, 28, 29, 38, 39, 46, 50, 50]. Others extend part segmentation to dynamic sequences by leveraging motion cues [0, 9, 59]. More recently, a line of research has evolved to jointly perform part segmentation and motion estimation from point cloud observations [0, 0, 35, 42]. MultiBodySync [02] introduces a differentiable permutation and segmentation module to iteratively find the optimal matching between point clouds. However, these methods often assume all parts are always completely visible. In contrast, we demonstrate that our method works on both complete and partial point cloud sequences.

Articulated object modeling. A major line of research reconstructs articulated shapes from images or videos with the help of informative visual features [20, 43, 51, 54, 56, 57]. However, some of these works focus on single object categories like humans [60, 40] or animals [22, 52, 54, 58, 64], where a kinematic structure is shared between all instances. For instance, GART [20] uses a categorical template model to recover the targets’ appearance from monocular videos. With strong categorical prior, these methods often focus on surface reconstruction and novel view synthesis, rather than part segmentation and motion analysis.

Some category-agnostic methods make assumptions about the number of moving parts [00, 03, 05, 09, 24, 47]. For example, Ditto [05] and PARIS [24] focus on objects with a single moving part given two observed articulated states. More recent works aim to generalize to arbitrary articulated objects. Watch-It-Move [56] models part poses and surfaces with ellipsoids and signed-distance functions (SDFs), which are optimized via volumetric rendering [48]. Then the underlying kinematic structure is inferred from the estimated part poses.

The closest work is Reart [26], which proposes a two-step optimization approach: a relaxed model with independent part poses and segmentation is first fitted to the observed 4D point cloud without any kinematic constraints. Then the underlying kinematic structure is estimated from the relaxed model. However, Reart selects a canonical time step and fits a MLP to segment points at this time step. Therefore, their segmentation model does not generalize to point clouds at other time steps, and the performance is sensitive to the chosen canonical frame. In contrast, we model the surface point distribution and part motion with 3D Gaussians, allowing us to segment point clouds at all time steps.

3 Method

Our goal is to estimate rigid part segmentation, kinematic structure and joint states from a sequence of K 3D point clouds $\mathcal{X} = \{\mathbf{X}^k\}_{k \in 1, \dots, K}$, where each point cloud $\mathbf{X}^k = [x_1^k, \dots, x_n^k, \dots, x_N^k]$ consists of N points in \mathbb{R}^3 sampled from the surface of an articulated object. Each point x belongs to one of the rigid parts of the object. Note that each point cloud \mathbf{X}^k is arbitrarily sampled at every time step k , therefore point correspondences do not exist in \mathcal{X} , since the corresponding points of x_i^k might not be sampled in the other time steps.

To estimate an articulated model from the given set of point cloud \mathcal{X} , we propose an optimization approach that consists of 3 steps. First, we optimize m 3D Gaussians independently where each Gaussian represents the point distribution and motion of a single rigid part (Section 3.1). Then we build a kinematic tree by adding edges between part pairs whose relative poses are close to 1-DOF motion (Section 3.2). Finally, the joint parameters of the kinematic tree are fine-tuned in a kinematic chain-aware fashion (Section 3.3).

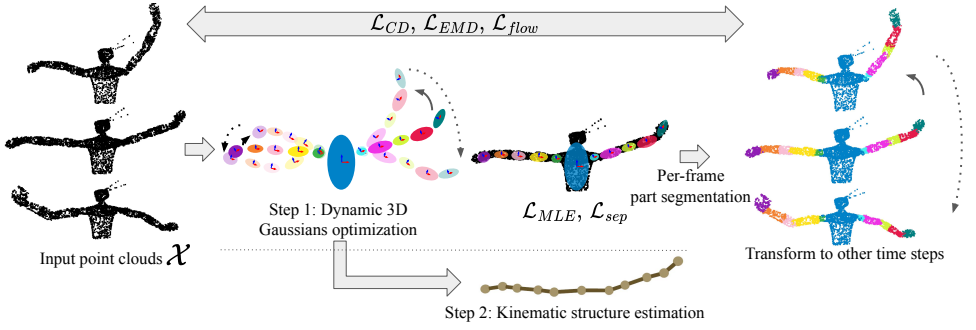


Figure 2: Our optimization pipeline. In each iteration, we sample a point cloud from \mathcal{X} uniformly at random, and optimize the Gaussian parameters at that time step by minimizing \mathcal{L}_{MLE} and \mathcal{L}_{sep} to maximize the log-likelihood of the observed point cloud, and ensure each Gaussian represents a single rigid part. Then we assign points to the Gaussians with the smallest Mahalanobis distance. Finally, we transform the segmented point cloud to other time steps with the corresponding Gaussian poses, and enforce similarity with the observed point clouds at those time steps.

3.1 Step 1: Modeling rigid parts with dynamic 3D Gaussians

Gaussian parametrization Each Gaussian G is defined by a full 3D covariance matrix Σ and center μ in the world frame: $G(x) = \frac{1}{(2\pi)^{n/2}|\Sigma|^{1/2}} \exp(-\frac{1}{2}(x - \mu)^T \Sigma^{-1}(x - \mu))$. The covariance matrix Σ is decomposed into a diagonal scaling matrix S and rotation R : $\Sigma = RS(RS)^T$. This representation allows independent optimization of the three factors for each Gaussian: a center $\mu \in \mathbb{R}^3$, scale $s \in \mathbb{R}^3$, and rotation matrix $R \in SO(3)$ represented with the 6D representation [63]. Moreover, the transformation $T \in SE(3)$ that transforms points from the Gaussian local frame to the observed point cloud frame (the world frame) can be defined as: $T = \begin{bmatrix} R & \mu \\ 0 & 1 \end{bmatrix}$. For each G to model the part motion over K time steps, we optimize K different R and μ while sharing the same s across all time steps. We denote the i -th Gaussian at the k -th time step as G_i^k , defined by R_i^k , μ_i^k , and s_i , with the associated part pose T_i^k .

Rigid part segmentation and point transformation We design the Gaussians to simultaneously encode both motions and point distributions of the rigid parts, allowing us to perform part segmentation without extra parameters. Given a 3D point x^k at time k , part segmentation is naturally achieved by selecting the Gaussian with the smallest Mahalanobis distance:

$$f(x^k) = \arg \max_{i \in \{1, \dots, m\}} (-\mathcal{M}(x^k, G_i^k)) \quad (1)$$

where \mathcal{M} is the squared Mahalanobis distance: $(x^k - \mu_i^k)^T \Sigma_i^{k-1} (x^k - \mu_i^k)$. To maintain differentiability during optimization, we replace $\arg \max$ with the Gumbel-Softmax trick [14, 53].

With our representation, point cloud X^k can be transformed from time k to time t :

$$\mathcal{H}_{k \rightarrow t} = \hat{X}^t = \{T_{f(x)}^t \cdot T_{f(x)}^k{}^{-1} \cdot \begin{bmatrix} x \\ 1 \end{bmatrix} \mid x \in X^k\} \quad (2)$$

The points are first transformed to the local frames of the estimated parts, then transformed back to the world frame with the part poses at other time steps. Moreover, we can fuse the

observed point clouds from all time steps to a single time step t after transforming to the same object pose: $\bigcup_{k=1}^K \mathcal{H}_{k \rightarrow t}$. We find this fusion ability critical, especially when handling point clouds with occlusions, since it allows us to gather information from all time steps.

Gaussian optimization The Gaussian parameters are optimized in an analysis-by-synthesis fashion as illustrated in Fig. 2. In every iteration, we sample a point cloud X^k from \mathcal{X} uniformly at random and perform a gradient step to minimize the loss: $\mathcal{L} = \lambda_{MLE} \mathcal{L}_{MLE} + \lambda_{sep} \mathcal{L}_{sep} + \lambda_{CD} \mathcal{L}_{CD} + \lambda_{EMD} \mathcal{L}_{EMD} + \lambda_{flow} \mathcal{L}_{flow}$. The goal is to enforce all m Gaussians to jointly model the observed point distributions while individual Gaussian represents a single rigid part. Moreover, X^k at time step k should be similar to any other point cloud X^t after being transformed with the corresponding Gaussian poses. Next, we detail each loss term:

Maximum likelihood loss: Given X^k , \mathcal{L}_{MLE} optimizes the Gaussian parameters to maximize the log-likelihood of the observed points. This loss is similar to the M step in the EM algorithm [54] for fitting a Gaussian Mixture Model (GMM) [40]. However, unlike standard GMMs, we enforce equal weights for all Gaussians to ensure that each Gaussian represents a single rigid part, while the overall Gaussians cover the entire point cloud.

$$\mathcal{L}_{MLE} = - \sum_{n=1}^N \log \left(\sum_{i=1}^m G_i^k(x_n^k) \right) \quad (3)$$

Separation loss: To ensure that each Gaussian represents a single rigid part, we apply \mathcal{L}_{sep} to avoid any two Gaussians being too close or overlap with each other.

$$\mathcal{L}_{sep} = \frac{1}{m} \sum_{i=1}^m \exp(-\alpha \cdot \min_{j \neq i} (\mathcal{M}(\mu_j^k, G_i^k))) \quad (4)$$

where α controls the minimum Mahalanobis distance between the center of a Gaussian to another Gaussian distribution. Larger α allows the Gaussians to be closer with each other.

Chamfer distance: Given one observed point cloud X^k , we can transform the points to all time steps $\{\mathcal{H}_{k \rightarrow t} | t = [1, \dots, K]\}$. We apply \mathcal{L}_{CD} to enforce the transformed point clouds to match the observations at other time steps by minimizing the Chamfer distance.

$$\mathcal{L}_{CD} = \sum_{t=1}^K \left(\sum_{x \in \mathcal{H}_{k \rightarrow t}} \min_{y \in X^t} \|x - y\|_2^2 + \sum_{y \in X^t} \min_{x \in \mathcal{H}_{k \rightarrow t}} \|x - y\|_2^2 \right) \quad (5)$$

Earth-mover distance: Similar to Chamfer distance, \mathcal{L}_{EMD} measures the similarity between two point clouds. Instead of finding the closest point as correspondence, \mathcal{L}_{EMD} finds the optimal matching between two point clouds by solving a bipartite matching problem [17].

$$\mathcal{L}_{EMD} = \sum_{t=1}^K \min_A \|A \mathcal{H}_{k \rightarrow t} - X^t\|_2^2 \quad (6)$$

where A denotes the permutation matrix solved using the linear assignment solver [9].

Flow loss: As demonstrated in [12, 24], flow prediction provides important cue regarding motion transition between point clouds. \mathcal{L}_{flow} encourages the point-wise 3D motion generated by our articulated model matches the prediction from a scene flow network.

$$\mathcal{L}_{flow} = \sum_{t=1}^{K-1} \left\| (X^{\hat{t}+1} - \hat{X}^t) - g(X^{t+1}, X^t; \hat{X}^t) \right\|_2^2 \quad (7)$$

where g is a pre-trained scene-flow network from [42, 46] that estimates the point-wise motion $g(X^{t+1}, X^t; \hat{X}^t)$ for all points in \hat{X}^t given two observed point clouds.

Another important factor is selecting an appropriate number of parts m during initialization. In most clustering algorithms, m is a hyperparameter chosen empirically using model selection criteria such as AIC for EM [44]. We follow a similar approach: we run our optimization with various values of m and choose the one that yields the minimum \mathcal{L}_{CD} after convergence. Additional detail about how this parameter affects our performance can be found in the supplementary material.

3.2 Step 2: Kinematic tree estimation

Given the predicted parts and motions, we adapt a scheme similar to [46, 36] for estimating the kinematic tree where each edge connects two parts with 1-DOF relative motion. We briefly outline the process here and provide more detail in the supplementary material.

If two parts form a parent-child pair in the kinematic tree, they must be spatially close, and their relative poses at all time steps should share the same rotation or translation axis. These two properties are measured with $\mathcal{L}_{spatial}$ and \mathcal{L}_{1-DOF} , respectively. For part i and j , $\mathcal{L}_{spatial}$ measures the shortest Euclidean distance between any pair of points: $\mathcal{L}_{spatial} = \min_{x \in X_i} \min_{y \in X_j} \|x - y\|_2^2$, where X_i and X_j denote the points that are segmented as the i -th and j -th part respectively. \mathcal{L}_{1-DOF} measures how well the relative motion between two parts

can be approximated by a 1-DOF relationship: $\mathcal{L}_{1-DOF} = \sum_k \left\| (\mathbf{O}_i^{k-1} \cdot \mathbf{O}_j^k) \cdot \mathbf{S}_{ij}^{k-1} - \mathbf{I} \right\|_F^2$,

where \mathbf{I} denotes the identity matrix. Here, $\mathbf{O}_i^k = \mathbf{T}_i^{k+1} \cdot \mathbf{T}_i^{k-1}$ is the motion of part i in the world frame between consecutive time steps. Hence, $(\mathbf{O}_i^{k-1} \cdot \mathbf{O}_j^k)$ calculates the relative motion of the two parts. \mathbf{S}_{ij}^k is the approximated 1-DOF relative motion between the two parts, considering their relative poses across all time steps. Essentially, \mathcal{L}_{1-DOF} measures the deviation of the observed relative motion from the approximated ideal 1-DOF motion.

Before constructing the kinematic tree, we first merge parts that are spatially close and their relative motion is close to static across all time steps. Then we compute pairwise $\mathcal{L}_{spatial}$ and \mathcal{L}_{1-DOF} between the remaining parts after merging. Finally, the kinematic tree is built by solving the minimum spanning tree problem (MST) [5] such that the total loss: $\lambda_{spatial} \mathcal{L}_{spatial} + \lambda_{1-DOF} \mathcal{L}_{1-DOF}$ of all edges in the tree is minimized.

3.3 Step 3: Joint parameters fine-tuning with kinematic constraints

Finally, the kinematic chain is constructed by first setting the part with the least motion across all time steps as the root node, followed by traversing outward to all leaf nodes to build the parent-child relationships. Joint parameters are then estimated by projecting Gaussian poses onto the chain, approximating 1-DOF screw parameters [52, 45] for each parent-child pair. These parameters are further refined via forward kinematics by minimizing \mathcal{L}_{CD} and \mathcal{L}_{EMD} .

4 Experiments

We evaluate our method on part segmentation, motion estimation, and re-articulation accuracy in Section 4.2. We then assess segmentation performance on a larger dataset of daily

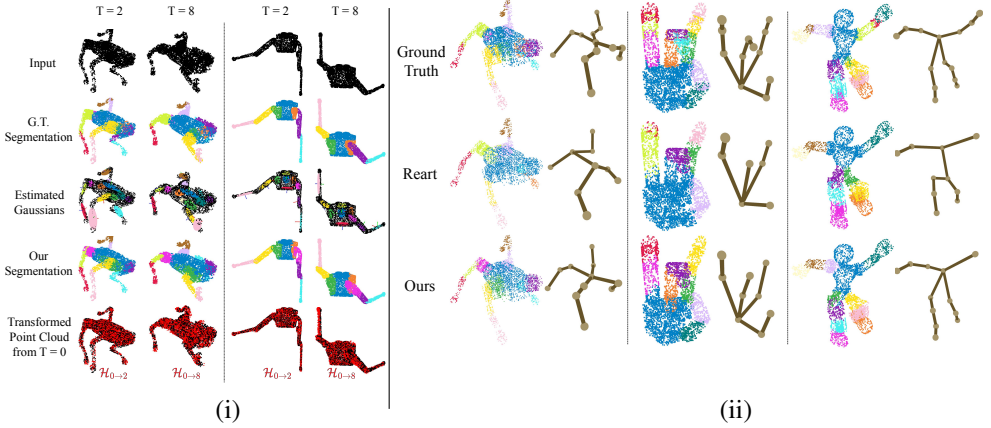


Figure 3: Qualitative results on the RoboArt dataset. (i) The third row shows our estimated Gaussians overlaid with the input point cloud (black). Segmentation results in the fourth row are obtained by assigning the points to the closest Gaussians, followed by the merging process in Section 3.2. The last row demonstrates motion quality by overlapping the observed point cloud at the current time (black) with points transformed from $T = 0$ (red), showing that the motion is well reconstructed even though they are two different point sets. (ii) Compared to Reart [76], our method is able to capture smaller parts more faithfully, for instance, the knuckles of the robot hand, leading to more accurate kinematic tree estimation.

objects in Section 4.3. Additionally, we create challenging datasets with occlusions by considering point visibility and demonstrate our method’s capability of handling noisy data in Section 4.4, even when some parts are completely occluded in some time-steps.

4.1 Experimental Setup

Datasets: Experiments are conducted on two main datasets: the **RoboArt** dataset [76], containing robot instances with up to 15 articulated parts and diverse kinematic structures (e.g., robot fingers, quadrupeds), and the **Sapien** dataset [4, 65], which includes 720 test sequences across 20 categories of daily objects. Note that the point clouds are arbitrarily resampled at every time step. To test robustness to occlusions, we generate two RoboArt variants: **Partial-RoboArt**, where only self-occlusion within each rigid part is considered (ensuring all parts remain partially visible), and **Occluded-RoboArt**, where we simulate real occlusions by removing points not visible from an arbitrarily sampled camera at each time step [4, 65], making some parts completely invisible in certain frames.

Metrics: **Reconstruction Error** and **Flow Error** [4, 76] measures the mean squared error (MSE) and point flow difference between point cloud sequences transformed with the ground truth vs. estimated parameters. **Rand Index (RI)** [4, 76] measures segmentation accuracy by calculating the pairwise agreement between the ground truth and predicted part label. **Tree Edit Distance** [57, 60] measures how close the predicted kinematic tree is to the ground truth tree. Finally, **Reanimate Error** [76] measures the MSE between the unseen articulated point clouds and the predicted reanimated point clouds to unseen poses.

Method	Recons Error↓	Rand Index↑	Tree Edit Distance↓	Reanimate Error↓	Flow Error↓
MultiBodySync [12]	4.76	0.70	6.6	9.72	3.42
WatchItMove [26]	12.77	0.78	6.6	7.43	8.42
Reart [26]	1.26	0.86*	2.9	3.66	0.57
Ours†	1.17	0.90	2.7	-	0.96
Ours	0.88	0.90	2.7	2.93	0.48

Table 1: Results on the RoboArt test set. † denotes running our method without kinematic parameter fine-tuning (Section 3.3). * Note that Reart evaluates their segmentation performance only on a single canonical frame, while we evaluate our method on all frames.

Method	Flow Error↓	Multi-scan RI↑	Per-scan RI↑
PWC-Net [53]	6.20	-	-
PointNet++ [38]	-	0.62	0.65
MeteorNet [12]	-	0.59	0.60
Deep Part [59]	5.95	0.64	0.67
NPP [8]	21.22	0.63	0.66
MultiBodySync [12]	5.03	0.76	0.77
Reart [26]	4.79	0.79	0.79
Ours	4.63	0.79	0.81
Ours*	4.58	0.82	0.83

Table 2: Results on the Sapien dataset. *denotes selecting the best result among the three initial parameters ($m = 3, 5, 7$).

4.2 Result on modeling articulated objects

We visualize the estimated 3D Gaussians in Fig. 3-(i), showing that each Gaussian follows the motion of its rigid part across time. We evaluate the estimated motion qualitatively in the last row. Despite the input point cloud sequence is sampled arbitrarily at each time step, the union of the observed and the transformed point clouds cover the object surface faithfully.

As shown in Table 1, our method outperforms existing approaches in all metrics on the RoboArt test set. Unlike correspondence-based methods [12, 26], which may fail when correspondences do not exist, our method models each rigid part as a 3D Gaussian and enforces similarity in point distributions across time for points belonging to the same part. As demonstrated in Fig. 3-(ii), this enables finer motion capture and more accurate segmentation of small parts, such as the knuckles of the robot hand or humanoid’s shoulder, which the baseline fails to achieve. In this experiment, we run our method with m from 10 to 15 for each instance and select the one with the least \mathcal{L}_{CD} after optimization. Similar process is employed in existing methods, for example, Reart [26] determines the canonical frame by performing multiple optimizations with different time step as the canonical frame and selecting the one with the lowest loss after convergence. Notably, Reart segments points only in the canonical time step, while our method is capable of segmenting points across all frames. Even when segmentation performance is evaluated over all time steps, as opposed to Reart’s single-frame segmentation, our method achieves better result, as presented in Table 1.

4.3 Result on segmenting object parts

We further evaluate the performance on part segmentation and flow prediction with the Sapien dataset (Fig. 4), which contains man-made objects with fewer articulated parts than RoboArt. Therefore we run our method with $m = 3, 5, 7$ as the number of part initialization. In addition to Per-scan RI, which evaluates segmentation frame-by-frame, we also include Multi-scan RI that assesses segmentation consistency across time. As shown in Table 2, optimization-based methods (e.g., Reart [26], MultiBodySync [12], Deep Part [59]) outperform feed-forward methods (e.g., PointNet++ [38], PWC-Net [53]) by trading off inference speed for better accuracy. Moreover, our per-frame segmentation performance outperforms MultiBodySync [12] that seeks to find point correspondences and Reart [26] that solves part-segmentation in a single frame. We also present the upper bound of our performance in Table 2, by reporting the best result among the three initial m . We show that with a better parameter selecting criterion, the performance of our method can be further improved.

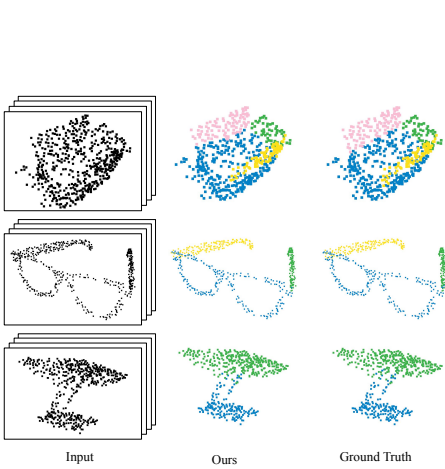


Figure 4: Qualitative result of our part segmentation on the Sapien dataset.

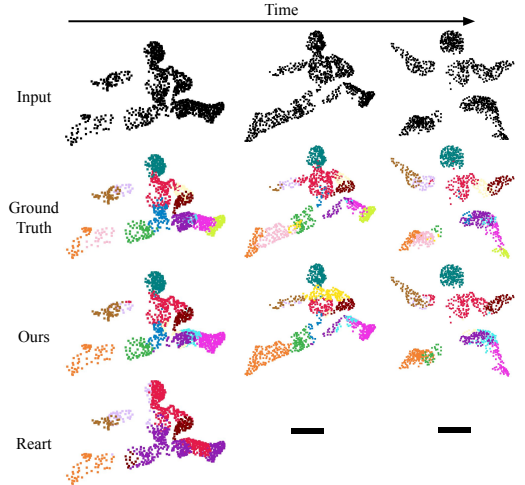


Figure 5: Qualitative results on Occluded-RoboArt. Our method separates the parts where the baseline fails.

4.4 Result on partial point clouds

We compare our method with Reart [26], which models part segmentation with a coordinate-based MLP, on two challenging datasets: Partial-RoboArt and Occluded-RoboArt. These datasets simulate real-world scenarios with occlusions, where not all parts are fully visible across time. Both methods are initialized with the same number of parts ($m = 20$). To handle missing points, we modify \mathcal{L}_{CD} and \mathcal{L}_{EMD} to compute the one-directional matching from the observed point cloud X^t to the fused point cloud from other time steps: $\bigcup_{k=1, k \neq t}^K \mathcal{H}_{k \rightarrow t}$. Details are provided in the supplementary material.

In Partial-RoboArt, all parts are partially observed across time, while some parts are fully missing in some frames in Occluded-RoboArt. As shown in Table 3, both methods perform worse when there are more missing points, while our method is less affected. Fig. 5 shows that our method separates parts more reliably than Reart. However, due to missing information, our method can produce noisy or inconsistent segmentation (e.g., the yellow part in the middle frame of the humanoid). This can happen when our method accidentally fits multiple Gaussians to different portions of that rigid part. Notably, Reart’s reliance on single-frame segmentation makes it more vulnerable when points do not exist in its selected canonical frame but appear in other time steps. This experiment highlights the advantages of considering point distribution of the rigid parts, and demonstrates that our method is more robust to occluded point clouds or points that do not completely cover the object surface.

4.5 Ablation studies

We conduct an ablation study to evaluate the effect of each loss term. As shown in Table 4, all components are essential. Among the point cloud reconstruction losses, \mathcal{L}_{EMD} and \mathcal{L}_{flow} , are particularly important, since they consider global point matching and motion accuracy. In contrast, \mathcal{L}_{CD} has less impact, which is due to its nearest-neighbor matching can easily result in incorrect correspondences. Moreover, \mathcal{L}_{MLE} significantly affects the performance

	Partial-RoboArt		Occluded-RoboArt	
	Reart [14]	Ours	Reart [14]	Ours
Recons Error ↓	4.65	1.99	7.66	2.68
Cano Frame RI ↑	0.78	0.85	0.75	0.85
Mean RI ↑	-	0.85	-	0.83
Flow Error ↓	2.64	1.26	4.73	1.74
Tree Edit Distance ↓	5.5	4.8	6.3	5.4

Table 3: Results on Partial-RoboArt and Occluded-RoboArt test set. Both datasets consist of point clouds with missing points, while Occluded-RoboArt has more missing parts. Result shows that Reart suffers more when there are more missing points, while our method is less sensitive to missing information.

Loss terms	Recons Error↓	Rand Index↑	Flow Error↓	Tree Edit Distance↓
w/o \mathcal{L}_{MLE}	3.03	0.81	1.90	6.25
w/o \mathcal{L}_{sep}	1.45	0.88	1.21	4.0
w/o \mathcal{L}_{CD}	1.51	0.87	1.14	4.0
w/o \mathcal{L}_{EMD}	10.04	0.75	6.70	6.5
w/o \mathcal{L}_{flow}	14.52	0.86	16.19	4.5
Ours	1.26	0.89	1.05	2.75

Table 4: Ablation study on RoboArt validation set. We evaluate the importance of each loss term by removing them one at a time.

of part segmentation, since it regularizes the Gaussians to cover the observed point clouds by enforcing equal weights. Without this loss, we observe that the model tends to ignore smaller rigid parts by using a larger Gaussian to approximate the motion of several neighboring smaller parts.

5 Conclusion

We presented a novel optimization approach to model arbitrary articulated objects from raw point cloud sequences. Our method jointly estimates per-frame part segmentation, part poses, and the kinematic structure with joint parameters, enabling re-articulation to unseen poses. By modeling rigid parts as point distributions, our method outperforms existing methods that solely rely on point correspondences on established benchmarks. Moreover, we created datasets that emulate real-world scenarios by considering viewpoint occlusions. Experiments showed that our method is more robust to missing points compared to past works, even when some parts are completely occluded in some frames. Notably, our segmentation achieves up to a 5% improvement over the SoTA on existing datasets, and a 13% improvement under partial observations. However, our method may fail when a large portion of the object is not seen across multiple frames. One possible solution is to apply a motion-aware generative model to fill in the missing information, which we leave for future work.

Limitations. As presented, our method requires the number of clusters m to be given as input. Although we propose a decision criterion for choosing the best m from multiple initializations, this requires additional computation time. A better solution, which we plan to explore in the future, could be to train a network for estimating the number of clusters. Additionally, our method assumes that the kinematic structure is acyclic and the parent-child part pairs exhibit 1-DOF relative motion. While these assumptions hold for many real-world objects, the kinematic tree estimation module needs to be generalized when these assumptions fail.

Acknowledgment. This work was funded in part by the National Research Foundation of Korea (NRF) grant (MSIT) No. RS-2024-00462874.

References

- [1] Ben Abbatematteo, Stefanie Tellex, and George Konidaris. Learning to generalize kinematic models to novel objects. In *Proceedings of the 3rd Conference on Robot Learning*, 2019.
- [2] Hameed Abdul-Rashid, Miles Freeman, Ben Abbatematteo, George Konidaris, and Daniel Ritchie. Learning to infer kinematic hierarchies for novel object instances. In *2022 International Conference on Robotics and Automation (ICRA)*, pages 8461–8467. IEEE, 2022.
- [3] Jun-Jee Chao, Selim Engin, Nicolai Häni, and Volkan Isler. Category-level global camera pose estimation with multi-hypothesis point cloud correspondences. In *2023 IEEE International Conference on Robotics and Automation (ICRA)*, pages 3800–3807. IEEE, 2023.
- [4] Xiaobai Chen, Aleksey Golovinskiy, and Thomas Funkhouser. A benchmark for 3d mesh segmentation. *Acm transactions on graphics (tog)*, 28(3):1–12, 2009.
- [5] Thomas H Cormen, Charles E Leiserson, Ronald L Rivest, and Clifford Stein. *Introduction to algorithms*. MIT press, 2022.
- [6] David F Crouse. On implementing 2d rectangular assignment algorithms. *IEEE Transactions on Aerospace and Electronic Systems*, 52(4):1679–1696, 2016.
- [7] Congyue Deng, Jiahui Lei, William B Shen, Kostas Daniilidis, and Leonidas J Guibas. Banana: Banach fixed-point network for pointcloud segmentation with inter-part equivariance. *Advances in Neural Information Processing Systems*, 36, 2024.
- [8] Nicolai Häni, Jun-Jee Chao, and Volkan Isler. 3d surface reconstruction in the wild by deforming shape priors from synthetic data. *arXiv preprint arXiv:2302.12883*, 2023.
- [9] David S Hayden, Jason Pacheco, and John W Fisher. Nonparametric object and parts modeling with lie group dynamics. In *Proceedings of the IEEE/CVF Conference on Computer Vision and Pattern Recognition*, pages 7426–7435, 2020.
- [10] Nick Heppert, Muhammad Zubair Irshad, Sergey Zakharov, Katherine Liu, Rares Andrei Ambrus, Jeannette Bohg, Abhinav Valada, and Thomas Kollar. Carto: Category and joint agnostic reconstruction of articulated objects. In *Proceedings of the IEEE/CVF Conference on Computer Vision and Pattern Recognition*, pages 21201–21210, 2023.
- [11] Cheng-Chun Hsu, Zhenyu Jiang, and Yuke Zhu. Ditto in the house: Building articulation models of indoor scenes through interactive perception. In *IEEE International Conference on Robotics and Automation (ICRA)*, 2023.
- [12] Jiahui Huang, He Wang, Tolga Birdal, Minhyuk Sung, Federica Arrigoni, Shi-Min Hu, and Leonidas J Guibas. Multibodysync: Multi-body segmentation and motion estimation via 3d scan synchronization. In *Proceedings of the IEEE/CVF Conference on Computer Vision and Pattern Recognition*, pages 7108–7118, 2021.

- [13] Ajinkya Jain, Rudolf Lioutikov, Caleb Chuck, and Scott Niekum. Screwnet: Category-independent articulation model estimation from depth images using screw theory. In *2021 IEEE International Conference on Robotics and Automation (ICRA)*, pages 13670–13677. IEEE, 2021.
- [14] Eric Jang, Shixiang Gu, and Ben Poole. Categorical reparametrization with gumble-softmax. In *International Conference on Learning Representations (ICLR 2017)*, 2017.
- [15] Zhenyu Jiang, Cheng-Chun Hsu, and Yuke Zhu. Ditto: Building digital twins of articulated objects from interaction. In *Proceedings of the IEEE/CVF Conference on Computer Vision and Pattern Recognition*, pages 5616–5626, 2022.
- [16] R JONKER and A VOLGENANT. A shortest augmenting path algorithm for dense and sparse linear assignment problems. *Computing (Wien. Print)*, 38(4):325–340, 1987.
- [17] Sagi Katz, Ayellet Tal, and Ronen Basri. Direct visibility of point sets. In *ACM SIGGRAPH 2007 papers*, pages 24–es. 2007.
- [18] Bernhard Kerbl, Georgios Kopanas, Thomas Leimkühler, and George Drettakis. 3d gaussian splatting for real-time radiance field rendering. *ACM Transactions on Graphics*, 42(4), July 2023. URL <https://repo-sam.inria.fr/fungraph/3d-gaussian-splatting/>.
- [19] Tianshu Kuai, Akash Karthikeyan, Yash Kant, Ashkan Mirzaei, and Igor Gilitschenski. Camm: Building category-agnostic and animatable 3d models from monocular videos. In *Proceedings of the IEEE/CVF Conference on Computer Vision and Pattern Recognition (CVPR) Workshops*, pages 6586–6596, June 2023.
- [20] Jiahui Lei, Yufu Wang, Georgios Pavlakos, Lingjie Liu, and Kostas Daniilidis. Gart: Gaussian articulated template models. In *Proceedings of the IEEE/CVF Conference on Computer Vision and Pattern Recognition*, pages 19876–19887, 2024.
- [21] Xiaolong Li, He Wang, Li Yi, Leonidas J Guibas, A Lynn Abbott, and Shuran Song. Category-level articulated object pose estimation. In *Proceedings of the IEEE/CVF conference on computer vision and pattern recognition*, pages 3706–3715, 2020.
- [22] Di Liu, Anastasis Sathopoulos, Qilong Zhangli, Yunhe Gao, and Dimitris Metaxas. Leopard: Learning explicit part discovery for 3d articulated shape reconstruction. In A. Oh, T. Naumann, A. Globerson, K. Saenko, M. Hardt, and S. Levine, editors, *Advances in Neural Information Processing Systems*, volume 36, pages 54187–54198. Curran Associates, Inc., 2023. URL https://proceedings.neurips.cc/paper_files/paper/2023/file/a99f50fb024a56d15f057a1830ed0a00-Paper-Conference.pdf.
- [23] Gengxin Liu, Qian Sun, Haibin Huang, Chongyang Ma, Yulan Guo, Li Yi, Hui Huang, and Ruizhen Hu. Semi-weakly supervised object kinematic motion prediction. In *Proceedings of the IEEE/CVF Conference on Computer Vision and Pattern Recognition*, 2023.
- [24] Jiayi Liu, Ali Mahdavi-Amiri, and Manolis Savva. Paris: Part-level reconstruction and motion analysis for articulated objects. In *Proceedings of the IEEE/CVF International Conference on Computer Vision*, pages 352–363, 2023.

- [25] Minghua Liu, Yinhao Zhu, Hong Cai, Shizhong Han, Zhan Ling, Fatih Porikli, and Hao Su. Partslip: Low-shot part segmentation for 3d point clouds via pretrained image-language models. In *Proceedings of the IEEE/CVF conference on computer vision and pattern recognition*, pages 21736–21746, 2023.
- [26] Shaowei Liu, Saurabh Gupta, and Shenlong Wang. Building rearticulable models for arbitrary 3d objects from 4d point clouds. In *Proceedings of the IEEE/CVF Conference on Computer Vision and Pattern Recognition*, pages 21138–21147, 2023.
- [27] Xingyu Liu, Mengyuan Yan, and Jeannette Bohg. Meteornet: Deep learning on dynamic 3d point cloud sequences. In *Proceedings of the IEEE/CVF International Conference on Computer Vision*, pages 9246–9255, 2019.
- [28] Xueyi Liu, Ji Zhang, Ruizhen Hu, Haibin Huang, He Wang, and Li Yi. Self-supervised category-level articulated object pose estimation with part-level se (3) equivariance. In *The Eleventh International Conference on Learning Representations*, 2023.
- [29] Yongcheng Liu, Bin Fan, Shiming Xiang, and Chunhong Pan. Relation-shape convolutional neural network for point cloud analysis. In *Proceedings of the IEEE/CVF conference on computer vision and pattern recognition*, pages 8895–8904, 2019.
- [30] Matthew Loper, Naureen Mahmood, Javier Romero, Gerard Pons-Moll, and Michael J. Black. SMPL: A skinned multi-person linear model. *ACM Trans. Graphics (Proc. SIGGRAPH Asia)*, 34(6):248:1–248:16, October 2015.
- [31] Jonathon Luiten, Georgios Kopanas, Bastian Leibe, and Deva Ramanan. Dynamic 3d gaussians: Tracking by persistent dynamic view synthesis. In *2024 International Conference on 3D Vision (3DV)*, pages 800–809. IEEE, 2024.
- [32] Kevin M Lynch and Frank C Park. Modern robotics: Mechanics, planning, and control. 2017.
- [33] C Maddison, A Mnih, and Y Teh. The concrete distribution: A continuous relaxation of discrete random variables. In *Proceedings of the international conference on learning Representations*, 2017.
- [34] Todd K Moon. The expectation-maximization algorithm. *IEEE Signal processing magazine*, 13(6):47–60, 1996.
- [35] Neil Nie, Samir Yitzhak Gadre, Kiana Ehsani, and Shuran Song. Structure from action: Learning interactions for 3d articulated object structure discovery. In *2023 IEEE/RSJ International Conference on Intelligent Robots and Systems (IROS)*, pages 1222–1229. IEEE, 2023.
- [36] Atsuhiko Noguchi, Umar Iqbal, Jonathan Tremblay, Tatsuya Harada, and Orazio Gallo. Watch it move: Unsupervised discovery of 3d joints for re-posing of articulated objects. In *Proceedings of the IEEE/CVF Conference on Computer Vision and Pattern Recognition*, pages 3677–3687, 2022.
- [37] Mateusz Pawlik and Nikolaus Augsten. Efficient computation of the tree edit distance. *ACM Transactions on Database Systems (TODS)*, 40(1):1–40, 2015.

- [38] Charles Ruizhongtai Qi, Li Yi, Hao Su, and Leonidas J Guibas. Pointnet++: Deep hierarchical feature learning on point sets in a metric space. *Advances in neural information processing systems*, 30, 2017.
- [39] Guocheng Qian, Yuchen Li, Houwen Peng, Jinjie Mai, Hasan Hammoud, Mohamed Elhoseiny, and Bernard Ghanem. Pointnext: Revisiting pointnet++ with improved training and scaling strategies. *Advances in neural information processing systems*, 35:23192–23204, 2022.
- [40] Douglas A Reynolds et al. Gaussian mixture models. *Encyclopedia of biometrics*, 741 (659-663):3, 2009.
- [41] Javier Romero, Dimitrios Tzionas, and Michael J. Black. Embodied hands: Modeling and capturing hands and bodies together. *ACM Transactions on Graphics, (Proc. SIGGRAPH Asia)*, 36(6), November 2017.
- [42] Yahao Shi, Xinyu Cao, and Bin Zhou. Self-supervised learning of part mobility from point cloud sequence. In *Computer Graphics Forum*, volume 40, pages 104–116. Wiley Online Library, 2021.
- [43] Chaoyue Song, Jiacheng Wei, Chuan Sheng Foo, Guosheng Lin, and Fayao Liu. Re-act: Reconstructing articulated objects from a single video. In *Proceedings of the IEEE/CVF Conference on Computer Vision and Pattern Recognition*, pages 5384–5395, 2024.
- [44] Russell J Steele and Adrian E Raftery. Performance of bayesian model selection criteria for gaussian mixture models. *Frontiers of statistical decision making and bayesian analysis*, 2:113–130, 2010.
- [45] Stefano Stramigioli and Herman Bruyninckx. Geometry and screw theory for robotics. *Tutorial during ICRA*, 2001:75, 2001.
- [46] Hugues Thomas, Charles R Qi, Jean-Emmanuel Deschaud, Beatriz Marcotequi, François Goulette, and Leonidas J Guibas. Kpconv: Flexible and deformable convolution for point clouds. In *Proceedings of the IEEE/CVF international conference on computer vision*, pages 6411–6420, 2019.
- [47] Wei-Cheng Tseng, Hung-Ju Liao, Lin Yen-Chen, and Min Sun. Cla-nerf: Category-level articulated neural radiance field. In *2022 International Conference on Robotics and Automation (ICRA)*, pages 8454–8460. IEEE, 2022.
- [48] Peng Wang, Lingjie Liu, Yuan Liu, Christian Theobalt, Taku Komura, and Wenping Wang. Neus: Learning neural implicit surfaces by volume rendering for multi-view reconstruction. *Advances in Neural Information Processing Systems*, 34:27171–27183, 2021.
- [49] Yian Wang, Ruihai Wu, Kaichun Mo, Jiaqi Ke, Qingnan Fan, Leonidas Guibas, and Hao Dong. AdaAfford: Learning to adapt manipulation affordance for 3d articulated objects via few-shot interactions. 2022.
- [50] Yue Wang, Yongbin Sun, Ziwei Liu, Sanjay E Sarma, Michael M Bronstein, and Justin M Solomon. Dynamic graph cnn for learning on point clouds. *ACM Transactions on Graphics (tog)*, 38(5):1–12, 2019.

- [51] Fangyin Wei, Rohan Chabra, Lingni Ma, Christoph Lassner, Michael Zollhoefer, Szymon Rusinkiewicz, Chris Sweeney, Richard Newcombe, and Mira Slavcheva. Self-supervised neural articulated shape and appearance models. In *Proceedings IEEE/CVF Conference on Computer Vision and Pattern Recognition (CVPR)*, 2022.
- [52] Shangzhe Wu, Ruining Li, Tomas Jakab, Christian Rupprecht, and Andrea Vedaldi. Magicpony: Learning articulated 3d animals in the wild. In *Proceedings of the IEEE/CVF Conference on Computer Vision and Pattern Recognition*, pages 8792–8802, 2023.
- [53] Wenxuan Wu, Zhi Yuan Wang, Zhuwen Li, Wei Liu, and Li Fuxin. Pointpwc-net: Cost volume on point clouds for (self-) supervised scene flow estimation. In *European Conference on Computer Vision*, pages 88–107, 2020.
- [54] Yuefan Wu*, Zeyuan Chen*, Shaowei Liu, Zhongzheng Ren, and Shenlong Wang. CASA: Category-agnostic skeletal animal reconstruction. In *Neural Information Processing Systems (NeurIPS)*, 2022.
- [55] Fanbo Xiang, Yuzhe Qin, Kaichun Mo, Yikuan Xia, Hao Zhu, Fangchen Liu, Minghua Liu, Hanxiao Jiang, Yifu Yuan, He Wang, et al. Sapien: A simulated part-based interactive environment. In *Proceedings of the IEEE/CVF conference on computer vision and pattern recognition*, pages 11097–11107, 2020.
- [56] Gengshan Yang, Deqing Sun, Varun Jampani, Daniel Vlasic, Forrester Cole, Huiwen Chang, Deva Ramanan, William T Freeman, and Ce Liu. Lasr: Learning articulated shape reconstruction from a monocular video. In *CVPR*, 2021.
- [57] Gengshan Yang, Minh Vo, Natalia Neverova, Deva Ramanan, Andrea Vedaldi, and Hanbyul Joo. Banmo: Building animatable 3d neural models from many casual videos. In *CVPR*, 2022.
- [58] Chun-Han Yao, Wei-Chih Hung, Yuanzhen Li, Michael Rubinstein, Ming-Hsuan Yang, and Varun Jampani. Lassie: Learning articulated shape from sparse image ensemble via 3d part discovery. In *NeurIPS*, 2022.
- [59] Li Yi, Haibin Huang, Difan Liu, Evangelos Kalogerakis, Hao Su, and Leonidas Guibas. Deep part induction from articulated object pairs. *ACM Transactions on Graphics (TOG)*, 37(6):1–15, 2018.
- [60] Li Yi, Wang Zhao, He Wang, Minhyuk Sung, and Leonidas J Guibas. Gspn: Generative shape proposal network for 3d instance segmentation in point cloud. In *Proceedings of the IEEE/CVF conference on computer vision and pattern recognition*, pages 3947–3956, 2019.
- [61] Kaizhong Zhang and Dennis Shasha. Simple fast algorithms for the editing distance between trees and related problems. *SIAM journal on computing*, 18(6):1245–1262, 1989.
- [62] Qian-Yi Zhou, Jaesik Park, and Vladlen Koltun. Open3D: A modern library for 3D data processing. *arXiv:1801.09847*, 2018.

- [63] Yi Zhou, Connelly Barnes, Jingwan Lu, Jimei Yang, and Hao Li. On the continuity of rotation representations in neural networks. In *Proceedings of the IEEE/CVF conference on computer vision and pattern recognition*, pages 5745–5753, 2019.
- [64] Silvia Zuffi, Angjoo Kanazawa, David W Jacobs, and Michael J Black. 3d menagerie: Modeling the 3d shape and pose of animals. In *Proceedings of the IEEE conference on computer vision and pattern recognition*, pages 6365–6373, 2017.